

# Intrinsic speckle noise in in-line particle holography due to poly-disperse and continuous particle sizes

Philip J. Edwards<sup>a</sup>, P. R. Hobson<sup>b</sup> and G. J. Rodgers<sup>c</sup>

<sup>a</sup>IPES, Brunel University, Uxbridge, Middlesex, UB8 3PH, U.K.

<sup>b</sup>Electronic and Computer Engineering, Brunel University, Uxbridge, Middlesex, UB8 3PH, U.K.

<sup>c</sup>Mathematical Sciences, Brunel University, Uxbridge, Middlesex, UB8 3PH, U.K.

## ABSTRACT

In-line particle holography is subject to image deterioration due to intrinsic speckle noise. The resulting reduction in the signal to noise ratio (SNR) of the replayed image can become critical for applications such as holographic particle velocimetry (HPV) and 3D visualisation of marine plankton. Work has been done to extend the mono-disperse model relevant to HPV to include poly-disperse particle fields appropriate for the visualisation of marine plankton. Continuous and discrete particle fields are both considered. It is found that random walk statistics still apply for the poly-disperse case. The speckle field is simply the summation of the individual speckle patterns due to each scatter size. Therefore the characteristic speckle parameter (which encompasses particle diameter, concentration and sample depth) is also just the summation of the individual speckle parameters. This reduces the SNR calculation to the same form as for the mono-disperse case. For the continuous situation three distributions, power, exponential and Gaussian are discussed with the resulting SNR calculated. The work presented here was performed as part of the Holomar project to produce a working underwater holographic camera for recording plankton.

**Keywords:** In-Line Holography, Speckle noise, signal to noise ratio, poly-disperse, continuous, particle size distribution

## 1. INTRODUCTION

In-line holography is limited to the studies of small particles due to the inherent restrictions of the technique, however within this specialized field it has many advantages over off-axis holography. A good example is its experimental simplicity which includes low demands on both laser coherence and film resolution. The technique of 'Fraunhofer' in-line particle holography has been extensively used in particle sizing,<sup>1,2</sup> particle coordinate<sup>3</sup> and velocity measurements.<sup>4,5</sup>

In-line particle holography is not without its limitations. The replayed image suffers from speckle noise. This noise becomes a limiting factor when the particle density is high or the depth of the particle field results in a large number of particles within the illuminated volume. For the application of the recording of marine plankton it is necessary to know the bounding limits of particle density and particle size for a 'good' hologram to be recorded.

A well known rule for determining the likely quality of the image is the Royer criterion.<sup>6</sup> This attributes the image deterioration to beam obscuration. The ratio of the total cross sectional area of particles over the total illuminated area is called the shadow 'density'. The quality of the image is defined as 'good' when the shadow density is less than 1%, between 1% and 10% produces a 'marginal' hologram, and if the shadow density is greater than 10% the hologram is 'bad'. This criteria is very convenient to use, but gives no appreciation of the quantitative value of the signal to noise ratio or the nature of the physical process involved in the formation of speckle.

In their work on HPV Meng et al developed a theoretical description of the formation of speckle fields in in-line particle holography<sup>7</sup>. They suggest that the physical process that produces speckle noise is the interference between the diffraction fields of individual scatterers. The signal to noise ratio is defined as the quotient of the intensity of the real image and the standard deviation of the intensity of the speckle field. Within their region of

---

Philip Edwards: E-mail: Philip.Edwards@physics.org

interest, mono-disperse particles, density  $1-100 \text{ mm}^{-3}$  and particle diameter  $1-100 \mu\text{m}$ , their model agrees well with experiment.

Plankton are microscopic creatures that live in the oceans. There are many species of plankton and they typically range in size from tens to hundreds of microns. They tend to exist in colonies and each colony can consist of thousands of individual plankton. The typical size and density of the plankton can fall within the requirements for a good in-line hologram. The driving force behind this research is the Holomar collaboration.<sup>8</sup> The goal is to develop, construct and evaluate a fully functioning prototype underwater holographic plankton camera (need information and reference about in-line holographic recording of plankton). It will be deployed with a replay facility and software to do data analysis and image recognition. This camera will be used to study plankton in their natural oceanic environment. Unfortunately for the plankton colonies the assumption that the particle field can be considered as mono-disperse is no longer valid. Instead it is necessary when determining the expected SNR of a replayed image to take into account the poly-disperse nature of the particle field. This possibility of poly-disperse particle fields is not discussed by Meng et al,<sup>7</sup> and is the focus of the work presented here.

The SNR is calculated for both discrete and continuous particle fields without implicitly assuming that random walk statistics apply. A relationship is formed to facilitate the reconstruction in the laboratory using mono-disperse seeding particles, the SNR measured in experimental situations due to poly-disperse particle fields.

## 2. THEORY OF IN-LINE HOLOGRAPHY OF PARTICLE FIELDS.

The physical process that is responsible for the formation of speckle patterns in in-line particle holography is the interference between the diffraction fields of many individual scatterers. If the positions of all the scatterers were known then the speckle pattern would be deterministic, but due to the random nature of the position of the scatterers the pattern is best described statistically. Therefore a speckle pattern is only correctly described by this analysis if the number of scatterers is sufficiently high. The SNR of the replayed image is defined as the quotient of the signal which is the intensity of the real image field  $I_{\text{sig}}$  and the standard deviation of the speckle field in the replayed image  $\sigma_{\text{BN}}$ .

$$\text{SNR} = I_{\text{sig}}/\sigma_{\text{BN}} \quad (1)$$

The calculation of the SNR reduces to the problem of calculating the dependence of the intensity of both the real image field and the standard deviation of the speckle field to physical experimental parameters.

### 2.1. Hologram Recording

The particles are randomly distributed and each of diameter  $d$  illuminated by a collimated laser beam of wavelength  $\lambda$ . The depth of the particle field is  $L$ . The hologram  $H$  is recorded at a distance  $z \gg d^2/\lambda$  from all the particles

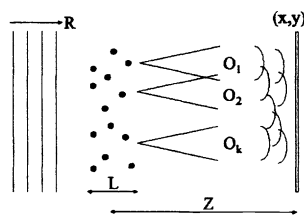


**Figure 1.** Scattering of light due to multiple particles in an in-line hologram recorded with a collimated illumination

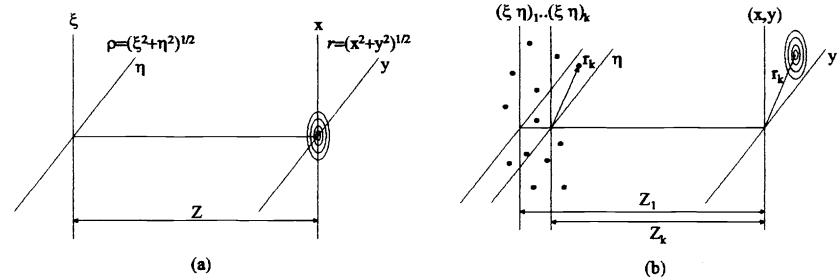


**Figure 2.** Coordinates for recording. (a) Single-particle case: a particle is centered in the origin of plane  $(\xi, \eta)$ , and its diffraction pattern is centered in the origin of the plane  $(x, y)$  at a distance  $z$  away; (b) multiple-particle case: the  $k^{\text{th}}$  particle is on the plane  $(\xi, \eta)_k$ , with location  $r_k$ , and its diffraction pattern centered at  $r_k$ , is observed on plane  $(x, y)$  at a distance  $z_k$ .

(This is the Fraunhofer far field condition. Practically one far field is sufficient). Light not scattered by the particles

is represented by the reference beam  $R$  and the scattered light by the object beam  $O$ . See Fig. 1 The resulting optical field at the recording plane  $(x, y)$  is given by

$$U_H(x, y) = R + O(x, y) = R + \sum_{k=1}^N o_k(x, y) \quad (2)$$

where  $o_k(x, y)$  is the scattered wave of the  $k^{\text{th}}$  particle. For simplicity the amplitude of the reference beam is taken as unity  $R = 1$ , and the intensity distribution at  $H$  is given by multiplying  $U_H(x, y)$  by its complex conjugate.

$$I_H(x, y) = U_H U_H^* = 1 + O^*(x, y) + O(x, y) + O(x, y)O^*(x, y) \quad (3)$$

The interference between the reference beam and the scattered light is given by  $(O + O^*)$ , and between individual scatters by  $OO^*$ . It is this cross term between the particles that appears as a random pattern if the number  $N$  of contributing scatterers is sufficiently high. The  $(O + O^*)$  term is the hologram pattern. The coordinate system used is shown in Fig. 2

When considering Fraunhofer in-line holography an object in the plane  $\xi\eta$  with transmittance  $1 - A(\xi, \eta)$  produces a Fraunhofer diffraction field  $U_H(x, y)$  on the recording plane  $(x, y)$ . The plane is located at a distance  $z$  from the object plane.  $A$  is the complement of amplitude transmittance function of the object. The field over the entire illuminated region can be described by the Fresnel approximation.

$$U_H(x, y) = -\frac{i}{\lambda z} \exp[i2\pi z/\lambda] \int_{-\infty}^{\infty} \int_{-\infty}^{\infty} [1 - A(\xi, \eta)] \times \exp\{i\pi[(x - \xi)^2 + (y - \eta)^2]/\lambda z\} d\xi d\eta \quad (4)$$

The far field condition  $(\xi^2 + \eta^2)/\lambda z \ll 1$  can be applied to the Fresnel approximation. This reduces the form of the Fresnel approximation equation to that resembling a Fourier integral. If a photographic recording is made of  $I_H(x, y)$  then this is known as a Fraunhofer hologram.

### 2.1.1. Single particle

Following the treatment of Meng et al<sup>7</sup> we initially consider a single spherical particle of diameter  $d$ . The object is modelled as an opaque disk, this is represented as a circ function in the  $(\xi, \eta)$  plane. This relates to an aperture function of  $A = \text{circ}(2|\rho - r_k|/d)$  where  $\rho$  is the radial coordinate of the disk. The subscript  $k$  is included to aid future multiple particle analysis. A particle is described by the index  $k$ , its radial location is at  $r_k = (a_k, b_k)$  and its distance from the hologram is  $z_k$ . For simplicity of integration the origins of the coordinate systems  $(x, y)$  and  $(\xi, \eta)$  are then moved to  $r_k$ . To represent the result of the integration in the same form as Eqn. (4) the following variables are defined as

$$C_k = \pi d^2 / (4\lambda z_k), \quad Q_k = \left\{ \frac{2J_1(\pi d|r - r_k|/\lambda z_k)}{(\pi d|r - r_k|/\lambda z_k)} \right\}, \quad \phi_k = (\pi|r - r_k|^2)/\lambda z_k + \pi/2 \quad (5)$$

$J_1$  is the first order Bessel function, and  $|r - r_k| = [(x - a_k)^2 + (y - b_k)^2]^{1/2}$ . Note that  $\lambda z_k C_k Q_k$  is the Fourier transform of the circ function. The object wave on the  $(x, y)$  plane can be written in terms of these variable as

$$O(x, y) = C_k Q_k \exp(i\phi_k)$$

and the intensity is equal to  $OO^*$

$$I_H(r) = 1 + 2C_k Q_k \cos(\phi) + C_k^2 Q_k^2$$

The second term in the expression for the intensity is known as the fringe signal. This corresponds to  $(O + O^*)$ . This is the signal which when replayed produces the real and virtual images of the original object(s) recorded.  $C_k$  is roughly the inverse of the far field number, its magnitude is typically of the order of  $10^{-2}$ . The last term,  $(OO^*)$ , is for the single particle case a halo with maximum intensity  $C_k^2$  and is therefore is negligible compared to the fringe signal.

### 2.1.2. Multiple particles: a bi-disperse particle field

The field at the recording plane due to two discrete sizes of scatterer is

$$O_{(x,y)} = \sum_{j'=1}^M C'_{j'} Q'_{j'} \exp [i\phi'_{j'}] + \sum_{j=1}^N C_j Q_j \exp [i\phi_j] \quad (6)$$

The average intensity of the speckle field is given as

$$\langle I \rangle = \left\langle \left[ \sum_{j'=1}^M C'_{j'} Q'_{j'} \exp [i\phi'_{j'}] + \sum_{j=1}^N C_j Q_j \exp [i\phi_j] \right] \times \left[ \sum_{k'=1}^M C'_{k'} Q'_{k'} \exp [-i\phi'_{k'}] + \sum_{k=1}^N C_k Q_k \exp [-i\phi_k] \right] \right\rangle \quad (7)$$

If  $L \ll Z$ , then  $C$  is taken as begin approximately constant for all scatterers.  $Q$  and  $\phi$  are independent random variables, therefore Eqn. (7) becomes

$$\begin{aligned} \langle I \rangle = & C'^2 \sum_{j'=1}^M \sum_{k'=1}^M \langle Q'_{j'} Q'_{k'} \rangle \langle \exp [i(\phi'_{j'} - \phi'_{k'})] \rangle + C' C \sum_{j'=1}^M \sum_{k=1}^N \langle Q'_{j'} Q_k \rangle \langle \exp [i(\phi'_{j'} - \phi_k)] \rangle + \\ & C C' \sum_{j=1}^N \sum_{k'=1}^M \langle Q_j Q'_{k'} \rangle \langle \exp [i(\phi_j - \phi'_{k'})] \rangle + C^2 \sum_{j=1}^N \sum_{k=1}^N \langle Q_j Q_k \rangle \langle \exp [i(\phi_j - \phi_k)] \rangle \end{aligned} \quad (8)$$

The only non zero terms in (8) are in the first expression. One the RHS when  $j' = k'$  and in the last expression when  $j = k$  therefore the average intensity reduces

$$\langle I \rangle = C^2 \sum_{j'=1}^M \langle Q'_{j'}{}^2 \rangle + C^2 \sum_{j=1}^N \langle Q_j{}^2 \rangle \quad (9)$$

Which is equivalent to:

$$\langle I \rangle = N C^2 \overline{Q_j^2} + M C'^2 \overline{Q'_{j'}^2} \quad (10)$$

### 2.1.3. Standard deviation

The square of the standard deviation is defined as  $\sigma^2 = \langle I^2 \rangle - \langle I \rangle^2$ . The average of the square of the intensity is

$$\begin{aligned} \langle I^2 \rangle = & \left( \sum_{j'=1}^M C'_{j'} \langle Q'_{j'} \rangle \langle \exp [i\phi'_{j'}] \rangle + \sum_{j=1}^N C_j \langle Q_j \rangle \langle \exp [i\phi_j] \rangle \right) \times \left( \sum_{k'=1}^M C'_{k'} \langle Q'_{k'} \rangle \langle \exp [-i\phi'_{k'}] \rangle + \right. \\ & \left. \sum_{k=1}^N C_k \langle Q_k \rangle \langle \exp [-i\phi_k] \rangle \right) \times \left( \sum_{l'=1}^M C'_{l'} \langle Q'_{l'} \rangle \langle \exp [i\phi'_{l'}] \rangle + \sum_{l=1}^N C_l \langle Q_l \rangle \langle \exp [i\phi_l] \rangle \right) \times \\ & \left( \sum_{m'=1}^M C'_{m'} \langle Q'_{m'} \rangle \langle \exp [-i\phi'_{m'}] \rangle + \sum_{m=1}^N C_m \langle Q_m \rangle \langle \exp [-i\phi_m] \rangle \right) \end{aligned} \quad (11)$$

Using the same analysis as before and assuming that  $N^2 \gg N$ ,  $M^2 \gg M$  and takes  $C$  to be constant

$$\langle I^2 \rangle = 2 \left( N^2 C^4 \overline{Q^2}^2 + 2 N M C^2 C'^2 \overline{Q^2} \overline{Q'^2} + M^2 C'^4 \overline{Q'^2}^2 \right) \quad (12)$$

So once again, as for the mono-disperse scatterer field<sup>7</sup> the standard deviation of the speckle field is equal to the mean of the speckle field.

$$\sigma = \langle I \rangle \quad (13)$$

This has shown from base principles that the standard deviation is equal to the mean when there are two discrete sizes of scatters present. An equivalent result can be achieved by considering the formation of speckle as a random

walk problem<sup>9</sup>. With the size of step taken being analogous to the diameter of the disks. The nature of the statistical probabilities arising from the random walk problem are not dependent on the size of step taken. So from this simple statement it can be seen that the size of the scatterer does not affect the statistical nature of the resultant speckle field.

An advantage of this treatment is that it shows that the statistics stay unchanged for multiple sizes of scatterers and therefore agrees with the statistics of random walk theory without having to assume this from the start. Also it derives an expression for the mean intensity, this can be measured experimentally and help to verify the results of the theory.

#### 2.1.4. Dependence of speckle intensity on the particle field

To calculate  $\sigma$  of the speckle intensity  $OO^*$  using equations (10) and (13), then the number of effective scatterers  $N$  contributing to an observable point P needs to be estimated as well as  $\overline{Q_k^2}$  which is the average of the Airy pattern intensity. As the diffraction of interest due to the experimental set up is essentially Fraunhofer diffraction the scattered energy is concentrated in the central lobe of the scatterer particle Airy pattern. Therefore the energy contributed to the speckle pattern by the side lobes is neglected at this stage. With this in mind the effective number of phasor elements contributing to the speckle at a point P can be determined by the number of scattering particles with central lobes overlapping at P. This is shown in Fig 3. The point P sees a conical region in the particle field

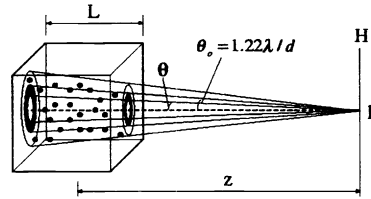


**Figure 3.** The Airy cone containing scatterers contributing to speckle at observation point P.

defined by a half angle

$$\theta_o = 1.22\lambda/d \cong \lambda/d$$

This angle corresponds to the first zero of the function  $J_1(x)/x$ . The number of particles in the Airy cone is

$$\begin{aligned} N &= (\pi/3) \rho \theta_o^2 \left[ (z + L/2)^3 - (z - L/2)^3 \right] \\ &= \pi \rho (\lambda^2 z^2 / d^2) (L + L^3 / 12z^2) \end{aligned} \quad (14)$$

For an experimental setup where  $z \gg L$  the second term in the above equation will be negligible compared to the first. So

$$N = \pi \rho \lambda^2 z^2 L / d^2 \quad (15)$$

Defining  $G \equiv NC^2$  and using  $C = \pi d^2 / (4\lambda z)$ , gives

$$G = \frac{\pi \rho \lambda^2 z^2 L}{d^2} \times \left[ \frac{\pi d^2}{4\lambda z} \right]^2 = \frac{\pi^3 \rho d^2 L}{16} \quad (16)$$

$G$  is the dimensionless speckle parameter.  $(d^2 \rho L)$  is equal to the shadow density and the equation above relates it to the physics of the scattering process.  $G$  represents the total scattering strength while  $C^2$  is the scattering strength of a single particle.

If the distribution of the disks is random then having a density  $\rho$  must correspond to the average number of disks contained in a volume. So the average intensity at the point P due to all the scatterers present in the conical volume

is calculated by taking a thin shell of differential angle  $d\theta$  at an angle  $\theta$ , with a range from zero to  $\theta_o$ . This average intensity is related to  $\overline{Q_k^2}$  by Equ (10) and results in

$$\overline{Q_k^2} = 2 \int_0^1 \{2J_1(\pi\alpha) / (\pi\alpha)\}^2 \alpha d\alpha \quad (17)$$

The integral can be calculated numerically and the result is  $0.335 \approx 1/3$ .  $\overline{Q_j'^2}$  is calculated in the same manner as  $\overline{Q_j^2}$  with  $G'$  defined as  $G' = MC'^2$ . The average intensity  $\langle I \rangle$  can be written as

$$\langle I \rangle = \frac{1}{3} (G + G') \quad (18)$$

The standard deviation can be expressed as

$$\sigma = \frac{\pi^3 L}{48} (d^2 \rho + d'^2 \rho') \quad (19)$$

## 2.2. Hologram Replay

When a hologram is reconstructed the illuminating plane wave is diffracted into four components. These components correspond to the terms in Eqn. (3). The real image is formed by the  $O^*$  term at a distance  $z$  behind the hologram, Fig 4. The  $O$  term produces a virtual image a distance  $Z$  in front of the hologram. The virtual image causes the illuminating plane wave to be diffracted much like in the recording process with the particle ensemble in place. Resulting in more speckle being created in the far field real image plane. But in this case the distance between the virtual and real image planes is  $2Z$ . The transmittance of the hologram is assumed to be

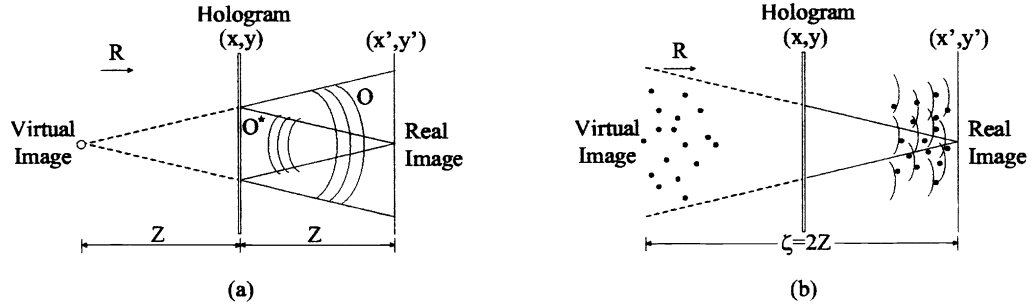


**Figure 4.** In line hologram reconstruction. (a) Single particle case, in which the virtual image is seen only as a weak, near spherical wave background in the real image plane  $(x', y')$ ; (b) multiple particle case: speckle arises from interference of waves from the virtual image of the particle ensemble.

$$t(x, y) = t_b - K [E(x, y) - E_b] \quad (20)$$

where  $t$  is the amplitude transmittance of the hologram,  $E$  is the exposure energy, and  $-K$  is the slope of the  $t - E$  curve of the film at a bias exposure  $E_b$ . As the recording intensity  $I_H(x, y)$  is normalized with respect to the plane wave illumination, it can be written that

$$E(x, y) = E_B I_H(x, y) \quad (21)$$

therefore  $t(x, y)$  can be rewritten as

$$t(x, y) = t_B - K E_b \Delta I_H(x, y) \quad (22)$$

where  $\Delta I_H(x, y)$  represents the intensity modulation,  $t_b$  is the transmittance due to exposure to just the plane wave illumination.

When replaying the hologram a plane wave is directed at the film. Immediately behind the film the transmitted field is proportional to  $t(x, y)$  and so

$$U_t(x, y) \propto B - [O^*(x, y) + O(x, y) + O(x, y)O^*(x, y)] \quad (23)$$

where

$$B \equiv \frac{t_B}{KE_B} \quad (24)$$

For simplicity in Eqn. (23) the proportionality is replaced with an equality. The resulting field at the real image plane  $(x', y')$  at a distance  $Z$  which is equal to the mean of  $Z_k$  is

$$U_R(x', y') = -\frac{i}{\lambda z} \exp[i2\pi z/\lambda] \int_{-\infty}^{\infty} \int_{-\infty}^{\infty} U_t(x, y) \times \exp\{i\pi[(x-x')^2 + (y-y')^2]/\lambda z\} dx dy. \quad (25)$$

When integrating the  $O^*$  and the  $O$  terms, these can be viewed as a sum of separate integrals associated with individual particles at various origin shifts  $r_k$  ( $k = 1, 2, \dots$ ). With the approximation of  $z_k \approx z$ , the hologram is

$$U_{sig} = \sum_k \text{circ}\left(\frac{|r' - r_k|}{d/2}\right) + \sum_{k'} \text{circ}\left(\frac{|r' - r_{k'}|}{d'/2}\right) \quad (26)$$

where  $|r' - r_k| = [(x' - a_k)^2 + (y' - b_k)^2]^{1/2}$ . This is because  $O^*$  produces the real image, which is formed in the replay plan. If no imperfections are present then the real image field produced by the  $O^*$  term is the same as the original object image field. From the  $O$  term the virtual image is formed in the same position as the original object. As for the  $O^*$  image the virtual image describes the same field as seen if the original objects were present. The result of this field on the replay plane is the same as if objects were actually present. The virtual field causes a speckle pattern to be formed on the replay field, but this time the distance is  $2z$ .

$$U_{sp1} = \sum_k^o C Q_k \exp[i\phi_k] + \sum_{k'}^p C' Q'_{k'} \exp[i\phi'_{k'}] \quad (27)$$

Here  $C$ ,  $Q_k$  and  $\phi_k$  are defined in the same manner as before. But now  $\phi_k$  has a constant phase delay of  $-\pi/2$ , not  $\pi/2$ . To be able to calculate the integral of the  $OO^*$  term the stationary phase approximation is applied<sup>10</sup>. The resulting integral shows that the interference pattern produced by a speckle pattern is itself a speckle pattern. The speckle field on the replay plan is a geometric propagation of the field transmitted through the specklegram. If this is considered statistically then the diffraction from a specklegram will be macroscopically similar to the field transmitted through the specklegram.

$$U_{sp2} = \frac{i}{\lambda z} \int_{-\infty}^{\infty} \int_{-\infty}^{\infty} OO^* \left(\frac{x}{\lambda z}, \frac{y}{\lambda z}\right) \times \exp\left\{\frac{i\pi z}{\lambda} [(x-x')^2 + (y-y')^2]\right\} dx dy \quad (28)$$

$$\cong -\frac{1}{4} OO^* \left(\frac{x}{\lambda z}, \frac{y}{\lambda z}\right)$$

Therefore the total reconstructed field at the replay plane can be written as

$$U_R(x', y') = B + U_{sig} + U_{sp1} + U_{sp2} \quad (29)$$

### 2.2.1. Evaluation of background noise

The signal of interest in the replay plane is described by equation (26). The background noise is then the sum of three coherent components. These are a constant phase  $\sqrt{I_c} \equiv B$  which is the transmitted plane wave and the two speckle fields,  $U_{sp1}$  and  $U_{sp2}$ . The total speckle field has an amplitude that is simply the sum of the individual speckle fields.

$$U_{sp} = U_{sp1} + U_{sp2} \quad (30)$$

Therefore the mean intensity of the total speckle field is

$$\langle I_{sp} \rangle = \langle U_{sp} U_{sp}^* \rangle \quad (31)$$

Substituting the expressions for  $U_{sp1}$  and  $U_{sp2}$  gives

$$\langle I_{sp} \rangle = \left\langle \left( \sum_k^o C Q_k \exp [i\phi_k] + \sum_{k'}^p C' Q'_{k'} \exp [i\phi'_{k'}] - \frac{1}{4} OO^* \right) \times \left( \sum_k^o C Q_k \exp [-i\phi_k] + \sum_{k'}^p C' Q'_{k'} \exp [-i\phi'_{k'}] - \frac{1}{4} OO^* \right) \right\rangle \quad (32)$$

Multiplying out Eqn. (32) and simplifying results in

$$\langle I_{sp} \rangle = \langle I_{sp1} \rangle + \langle I_{sp2} \rangle \quad (33)$$

where

$$\begin{aligned} \langle I_{sp1} \rangle &= \sum_{k'=1}^p C'^2 \langle Q'_{k'} \rangle + \sum_{k=1}^o C^2 \langle Q_k^2 \rangle \\ &= \frac{G}{3} + \frac{G'}{3} = \frac{1}{3}(G + G') \end{aligned} \quad (34)$$

and

$$\langle I_{sp2} \rangle = \frac{1}{16} \langle (OO^*)^2 \rangle \quad (35)$$

For the two disk problem since the background field is a random walk plus a constant phase. The random walk is the speckle noise, whilst the constant phase is the reference beam. The probability density function of the total background intensity  $I_{BN}$  is a modified Rician function<sup>11</sup>. The mean intensity is

$$\langle I_{BN} \rangle = \langle I_{sp} \rangle + I_c \simeq \frac{1}{3}(G + G') + B^2 \quad (36)$$

$$\sigma_{BN} = \frac{1}{3}(G + G') \left[ 1 + \frac{6B}{G + G'} \right]^{1/2} \quad (37)$$

$$\text{SNR} = \left\{ \frac{G + G'}{3} \left( 1 + \frac{6B}{G + G'} \right)^{1/2} \right\}^{-1} \quad (38)$$

The speckle pattern in the case of two different sizes of scatterer is simple the summation of the individual speckle patterns. The statistics of the speckle pattern remain unaltered. The results can be generalised to say that the speckle pattern due to a poly-disperse particle field will simply be the summation of the individual speckle fields and that the statistics of the speckle pattern will be the same as for the mono-disperse case.

### 3. SIMULATIONS OF THE DISCRETE THEORY

Simulations were performed to test the validity of the theoretical results for the discrete theory. The SNR ratio is dependent on the statistics of the speckle pattern. So the results of the theory rest on the correct theoretical description of the statistical nature of the speckle pattern. So it is this that is tested.

#### 3.1. Ideology of the Algorithm

The far field diffraction pattern due to scatterer is calculated and is then mapped onto the recording plane in random locations  $N$  times. Where  $N$  corresponds to the number of scatters present. The expression for the field due to one scatter is calculated and stored in an array. The mesh of the array is user defined. The size of the recording plane is also user defined, but the mesh is set to the same value as the scatter field array. For each scatter the scatter

field array is randomly placed within the recording plane array. Its values are added to that already present in the recording array. In this way the speckle noise due to  $N$  scatterers of uniform size is reproduced.

One of the assumptions of the paper is that only the central lobe of the Airy pattern contributes appreciable to the speckle pattern. To test this it is necessary to change the amount of the scatterer field used within the calculation. With this setup it is simply a matter of changing the size of the scatterer array. The larger the array, the more side lobes of the Airy pattern are included.

The global accuracy of the calculation can be controlled by increasing the mesh size of the scatterer field. But by increasing the mesh size by a factor of,  $c$  the number of calculations increasing by a factor of  $c^2$ . Therefore a compromise between accuracy and computing time is required when processing large fields.

For the situation were there are two sizes of discrete scatterers only minor alterations to the algorithm were required. Instead if just one scatterer field array, two scatterer field arrays of different sizes are defined of  $N$  and  $M$  elements. These are then randomly added to the recording plane array as before.

### 3.2. Details of Simulations

First simulations using mathematica v3 were run to see if the computational model would recreate the results predicted by the paper. So a mono-disperse particle field of 600 scatterers was chosen.

For the poly-disperse field the scatterers consisted of 500 small and 100 large scatterers. The large scatterers are twice as large as the small scatterers. Resulting in a total of 600 scatterers, the same as that for the mono-disperse case. The value of the numbers is rather arbitrary though a greater number of smaller scatterers was taken as this is the practically more realistic case with regards to plankton colonies.

### 3.3. Results of Simulations

The statistical results of the mono-disperse simulations, Fig 5 to 7 were compared to the expected results quoted in the paper<sup>7</sup> and those found in "Laser speckle and related phenomena"<sup>11</sup>. The simulation of the situation of

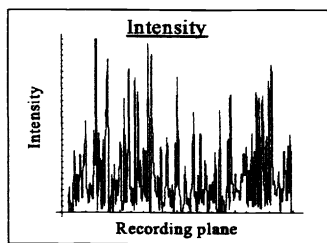


**Figure 5.** Intensity plot of 600 small scatterers.

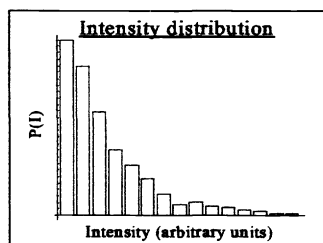


**Figure 6.** Intensity distribution Plot of 600 small scatterers.

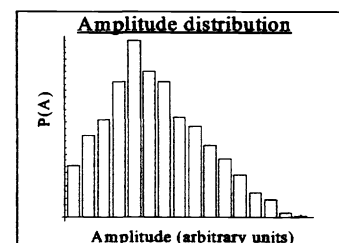


**Figure 7.** Amplitude distribution plot of 600 small scatterers

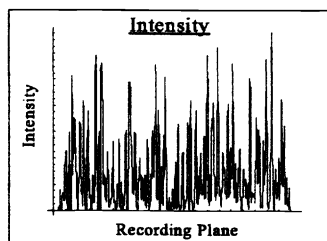


**Figure 8.** Intensity plot of 500 small and 100 large scatterers.

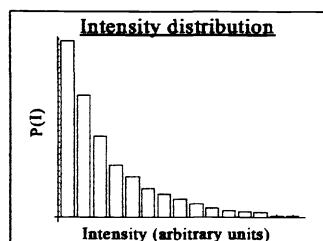


**Figure 9.** Intensity distribution plot of 500 small and 100 large scatterers

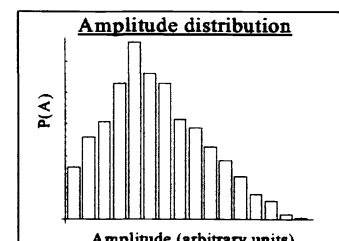


**Figure 10.** Amplitude distribution plot of 500 small and 100 large scatterers.

uniform scatter size gives good statistical agreement with the theory. The intensity distribution follows a negative exponential curve and the amplitude is Gaussian. The statistics of the poly-disperse case, Fig. 8 to 10 are consistent with predicted distributions.

#### 4. CONTINUOUS DISTRIBUTION OF SCATTERERS

It is more likely to have a wide range of plankton sizes in a volume of sea which would be best described by a continuous distribution rather than only having plankton at certain discrete sizes.

##### 4.1. Developing a Continuous Description

The continuous problem is constructed on the foundation of the discrete problem. Using the relationship  $\sum g(f) \equiv \int P(f)dfg(f)$  the equations for the discrete problem can be converted into relevant equations for the continuous case. The average amplitude at a particular point on the recording plane is given by

$$O(x, y) = \int P(C)CQ_c \exp [i\phi_c]dC \quad O^*(x, y) = \int P(C)CQ_c \exp [-i\phi_c]dC \quad (39)$$

Therefore the intensity is given by

$$I = OO^* = \int P(C)P(C')CC'Q_cQ_{c'} \exp [i(\phi_c - \phi_{c'})]dcd c' \quad (40)$$

The ensemble average of Eqs. (40) is non zero when  $c=c'$ , therefore

$$\langle I \rangle = \int P(C)^2 C^2 Q_c^2 dC \quad (41)$$

##### 4.2. Initial Verification of the Continuous Solution

In an attempt to verify the equation it is tested whether the continuous equation produces the same results for the situation where there is only one size of scatterer as produced by the discrete solution. The probability of finding a scatterer of size  $C$  is

$$P(C) = \sum_{j=1}^N \delta C C' \quad (42)$$

$$(43)$$

Placing this probability back into the continuous expression (41).

$$\langle I \rangle = \sum_{k=1}^N \sum_{j=1}^N \delta C_k C_j C_j^2 Q_{c_j}^2 = \sum_{j=1}^N C_j^2 Q_{c_j}^2 \quad (44)$$

This is the relationship derived by Meng et al.<sup>7</sup>

##### 4.3. Formulation of the General Continuous Solution Without Probability Function

Substituting the relationships given in (5) into Equ (41) gives

$$\langle I \rangle = \int_a^b P(C)^2 C \frac{J_1^2 \left[ 2\sqrt{\pi\lambda Z C} / \lambda Z \right]}{\pi\lambda Z} dC \quad (45)$$

When considering what values should be taken by the limits. It is important to consider one of the assumptions that the recording plate is always in the Far Field of all the objects. Therefore the greatest diameter of scatterer is determined by the Far Field condition,  $Z \gg d^2/\lambda$ . For practical In-Line particle holography one far field is sufficient. The minimum size is in practice finite, though here to it is simplified to zero.

$$\langle I \rangle = \frac{\lambda Z}{\pi} \int_0^{\pi/4} P(C)^2 C J_1^2 \left[ 2\sqrt{\pi\lambda Z C} / \lambda Z \right] dC \quad (46)$$

This is the general continuous solution, it requires the appropriate probability function.

#### 4.4. Probability Distributions

It is now necessary to consider what probability distributions are relevant. A rule of thumb is that the total volume taken up by each size of scatterer remains approximately constant. i.e. there are far more of smaller plankton than of larger varieties. This would give a relationship of the form  $P(d) \approx d^{-3}$ . Taking a more general power relationship, the parameter  $d$  is raised to some power  $n$ .

$$P(C)^2 = \left(\frac{4\lambda Z}{\pi}\right)^{-n} C^{-n} \quad (47)$$

Substitute this into the general continuous Eqn. (46) and simplifying the equation by make the substitution  $u = \sqrt{C}$

$$\langle I \rangle = 2 \times 4^{-n} \left(\frac{\lambda Z}{\pi}\right)^{-n+1} \int_0^{\pi/4} u^{-2n+3} J_1^2 \left[ \frac{2\sqrt{\pi\lambda Z}}{\lambda Z} u \right] du \quad (48)$$

This average intensity is the first step in calculating the SNR of the hologram due to a continuous distribution of scatterer size.

The above construction can be performed for both exponential and Gaussian distributions.

##### 4.4.1. Initial investigation of the behaviour of the average intensity with a power distribution

This is an investigation purely into the form of the result. Equ (48) is simplified to

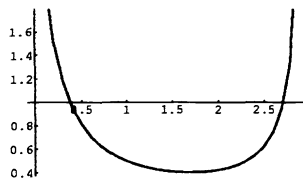


**Figure 11.** Graph showing the numerical integration (y-axis) of the average intensity integral (equation (49)) for power  $n$  (x axis).

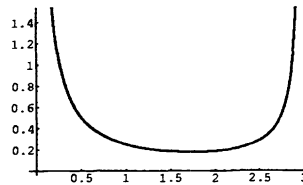


**Figure 12.** Graph showing the analytical integration of Eqn. (49) (y axis) for power  $n$  (x axis).

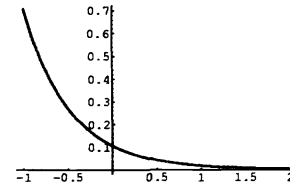


**Figure 13.** Graph showing the numerical solution (y-axis) of the average intensity integral for power  $n$  (x axis), including the Far field condition.

$$\langle I \rangle = \int_0^{\infty} u^{-n} J_1^2(u) du \quad (49)$$

The integration range was changed so it ranged from 0 to  $\infty$ . As a closed form solutions exist for this integral allowing the numerical algorithm developed for solving this integral over varying powers of  $n$  to be checked. The closed form solution for this integral is exists<sup>12</sup> and is plotted in Fig. 12. The analytical solution is only valid over the range 0 to 3. The result where the integral is numerically integrate using Mathematica is shown in Fig. 11. This is in very close agreement with the analytical result and shows the result of the integral diverging at the values of  $n$  of 0 and 3. The physical interpretation of this is that the distributions of the characteristic size of the scatterer  $d$  is only solvable for negative powers of  $n$  between 0 and 3. This is for the integrations limits 0 to  $\infty$ .

When the far field limit is considered with regards to scatterer size there is no longer a closed form solution, therefore the numerical algorithm is used with the upper limit changed in accordance to the far field condition. Fig. 13 show the plot of integral (49) with the new limits. Figure 13 suggest that as the power that the parameter  $d$  is raised to decreases the average intensity also decreases of the speckle pattern. In the figure the x axis shows  $-n$ , therefore a positive value on the x axis is in fact representing a negative value of  $n$ . The inverse is also true that as the power that the parameter  $d$  is raised to is increased the average intensity also increases. To achieve quantitative results from these calculations equation (48) must be used instead of equation (49). Once this has been calculated the SNR ratio of the hologram may be formulated. This is left as a further work.

## 5. CONCLUSIONS

We have shown using scalar diffraction theory that random walk statistics describe the speckle field due to poly-disperse particle fields. The resulting total speckle field is simply the sum of the speckle fields due to each scatterer size.

The SNR of distributions that are described by discrete groups of scatterer size can be calculated by extrapolating Eqn. (38). As for the mono-disperse situation the SNR is found to decrease with increasing particle concentration, volume depth and particle diameter. This is encapsulated in the speckle parameter  $G$ . An analytical solution exists for the continuous power distribution of scatterer size. Using the far field condition the range of power distributions over which the SNR can be calculated is increased. Numerical solutions for the exponential and Gaussian distributions have been calculated. The SNR for continuous distributions can be approximated by the discrete solution or the average intensity of the speckle field found by substituting the distribution into Eqn. (46). From the average intensity the SNR can be calculated.

A useful application of this work is to calculate the density and size of scatterer of a mono-disperse field required to replicate the SNR measured in a hologram of plankton. This would facilitate the reproduction of experimental conditions in the laboratory.

We believe that this work has relevance in the holographic recording of particle fields consisting of simultaneous scatterer sizes.

## REFERENCES

1. B. J. Thompson, "Holographic particle sizing techniques," *J. Phys E*(7), pp. 781–788, 1974.
2. P. D. S. L. Cartwright and B. J. Thompson, "Particle sizing using far-field holography: new developments," *Opt Eng* (19), pp. 727–733, 1980.
3. P. R. Hobson, "Precision coordinate measurement using holographic recording," *J. Phys E*(21), pp. 139–145, 1988.
4. R. A. B. J. D. Trolinger and W. M. Farmer, "Holographic techniques for the study of dynamic particles fields," *Appl. Opt* (8), pp. 957–961, 1969.
5. P. H. Malyak and B. J. Thompson, "Particle displacement and velocity measurement using holography," *Opt. Eng* (23), pp. 567–576, 1984.
6. H. Royer, "An application of high speed microholography: the metrology of fogs," *Nouv. Rev. Opt* 5, pp. 87–93, 1974.
7. F. H. Hui Meng, W. L. Anderson and D. D. Liu, "Intrinsic speckle noise in in-line particle holography," *J. Opt. Soc Am* 10, pp. 2046–2058, September 1993.
8. Watson J et al, "High-resolution in situ holographic recording and analysis of marine organisms and particles (holomar)," *Proc. Oceans* , pp. 1599–1603, 1998.
9. W. Feller, *An Introduction to Probability Theory and Its Application*, John Wiley and Sons, 1968.
10. G. A. Tyler and B. J. Thompson, "Fraunhofer holography applied to particle size analysis: a reassessment," *Opt* (23), pp. 688–700, 1976.
11. J. D. Goodman, *Statistical properties of laser speckle patterns*, ch. 2. in *Laser Speckle and Related Phenomena*, J. C. Dainty, ed. Springer-Verlag, Berlin, 1984.
12. I. S. Gradshteyn and I. M. Ryzhik, *Table of Integrals Series and Products*, Academic Press City London, 1994.